

AN ANATOMICAL MODEL FOR STREAMING POTENTIALS IN OSTEONS

S. R. POLLACK,* N. PETROV,† R. SALZSTEIN,* G. BRANKOV† and R. BLAGOEVA†

*Department of Bioengineering, University of Pennsylvania, Philadelphia, PA, U.S.A.

†Institute of Mechanics and Biomechanics, Bulgarian Academy of Sciences, Sofia, Bulgaria

Abstract—An anatomical model for streaming potentials in osteons is developed to characterize the electromechanical effect in bone. The model accounts for the microstructure of the osteon and is based upon first principles of electrochemistry, electrokinetics, continuum mechanics and fluid dynamics. Intra-osteonal potentials and their relaxation times are numerically evaluated. Many of the previously reported observations of potentials in osteons and across macroscopic specimens are explained for the first time in terms of an electrokinetic model. The cusp-like behavior of intra-osteonal potentials is explained, the dependence of the potentials on solution viscosity and conductivity is demonstrated, and insight is gained relative to the time dependence of stress generated potentials.

NOMENCLATURE

ρ	charge density in fluid
r	radial coordinate in channel
z^l	valence of ion species l
e	electronic charge
C^l	concentration of ion species l
C_o^l	equilibrium concentration of ion species l
ϕ	potential
k	Boltzmann's constant
T	absolute temperature
ϵ	dielectric permittivity of fluid
κ^{-1}	Debye length
Z	zeta potential
V	volume of lacuna
P	pressure in lacuna
P_o	initial pressure in lacuna
S	uniaxial stress
μ_1	shear modulus of bone matrix
K_1	bulk modulus of bone matrix
K_w	bulk modulus of fluid (water)
V_o	initial lacunar volume
n_i	number of channels for the i th lacuna
n	average number of channels per lacuna
R	radius of channel
L_i	length of channel
Q	volume flow rate
η	viscosity of fluid
K_{eff}	effective bulk modulus
τ_i	relaxation time
v	fluid velocity
j_{ei}	convective electrical current
N_i	number of lacunae at radius a_i
u	radial coordinate in osteon
h	length of osteon
J	conduction current density
σ	conductivity of bone-fluid system
E_u	radial component of electric field
q	charge
ϵ_s	dielectric permittivity of bone-fluid system
\bar{u}	Haversian canal radius

INTRODUCTION

When a time dependent load is applied to cortical bone, the deformation of the matrix produces flow of

the fluid that fills the porous fraction of bone (Piekarski and Munro, 1977). In the presence of a non-zero zeta potential (Eriksson, 1976; Gross and Williams, 1982), electrokinetic effects in the form of stress generated potentials (SGP's) result in accordance with Anderson and Eriksson's (1970) original proposals. It is the purpose of this work to develop an analytical expression for these stress generated potentials that takes into account the microstructure of an osteon and the properties of the fluid such as viscosity, ion concentration and conductivity.

Recent work in this field has indicated that electrical potentials observed during deformation of fluid filled bone may be of electrokinetic origin (Johnson *et al.*, 1980, 1982; Gross and Williams, 1982; Pienkowski and Pollack, 1983). This is not to say that piezoelectric-like effects do not occur. Rather, these authors conclude that both mechanisms are operative and, in dry bone, only the piezoelectric effect can be observed, while in fluid filled bone, the electrokinetic effects dominate.

This work will focus on SGPs generated within a fluid filled osteon and results will be compared to experimental work reported by Iannacone *et al.* (1979), Starkebaum *et al.* (1979), Gross and Williams (1982) and Pienkowski and Pollack (1983), who investigated intra-osteonal potentials using microelectrode methods or determined macroscopic SGP's using macroelectrode methods.

THEORY

Bone contains approximately 20% fluid by weight. This fluid fills the various channels of bone as well as the porous region within the bone matrix. The channels include the lacunae, canaliculi, Haversian canals and Volkmann's canals. The porous region within the matrix refers to the spaces surrounding the collagen-mineral matrix of bone and such spaces also contain the glycosaminoglycans. There is a wide variation in the dimensions of these spaces as shown in Table 1. This model will consider the flow in channels that are

Received September 1983; in revised form March 1984.

Table 1. Approximate sizes of fluid filled regions in bone

Region	Shape	Approximate size
(1) Lacuna	Ellipsoidal	5–10 μ (major ellipsoidal axis)
(2) Canaliculi	Cylindrical	0.2 μ diameter 10–40 μ length
(3) Haversian canal	Cylindrical	25–50 μ diameter 1000 μ length or longer
(4) Volkmann's canal	Cylindrical	25–50 μ diameter 200–500 μ length
(5) Pores in matrix	Irregular	Variable, on the order of 10–200 Å

connected to lacunae and 'drain' the lacunae when they are pressurized during deformation. The channels that actually radiate from the lacunae toward the cement line are assumed to be incorporated into lacunae lying at positions closer to the cement line. Of course, at or near the cement line, these channels are not accounted for and therefore these results will not explain data in this region.

The osteon is modelled as in Fig. 1. Following the method of Overbeek (1952), we calculate the equilibrium charge distribution in the fluid within cylindrically shaped channels, for the case of a monovalent ion system, such as NaCl or KCl, and in the absence of fluid flow. A step load, resulting in uniaxial stress, is then applied and a current density results from laminar convective flow in the channels due to compression (or expansion) of the lacunar space. The hydrodynamic pressure differential between the lacunae and the Haversian canal (taken to be open to atmospheric pressure or arterial pressure) is determined as a function of the deformation and the total convective flow in all channels is then determined. This convective current results in a radially dependent potential difference between the Haversian canal and the cement

line of the osteon. This potential difference causes a reverse conduction current and steady state is obtained when the conduction current equals the convective current. The electrical potential that exists when the steady state condition is met is called the streaming potential or electrokinetic potential (Shaw, 1969). This steady state streaming potential will be a function of the deformation, the properties of the fluid such as the viscosity and the electrical conductivity, the anatomical model of the osteon, and, of course, the local values of the zeta potential. This relationship is then compared to experimental results, published in the literature.

Equilibrium ion distribution in a cylindrical channel

Figure 2 shows a model of a channel connecting a lacunar space with a Haversian canal. Direct zeta potential measurements in bone by Eriksson (1976) and Gross and Williams (1982) clearly indicate the presence of an electrical double layer at the bone-fluid interface. Such double layers arise because a net surface charge is acquired on the surface of bone when in contact with fluid containing ions. The ion charge density ρ in the fluid is a function of the radius r and is

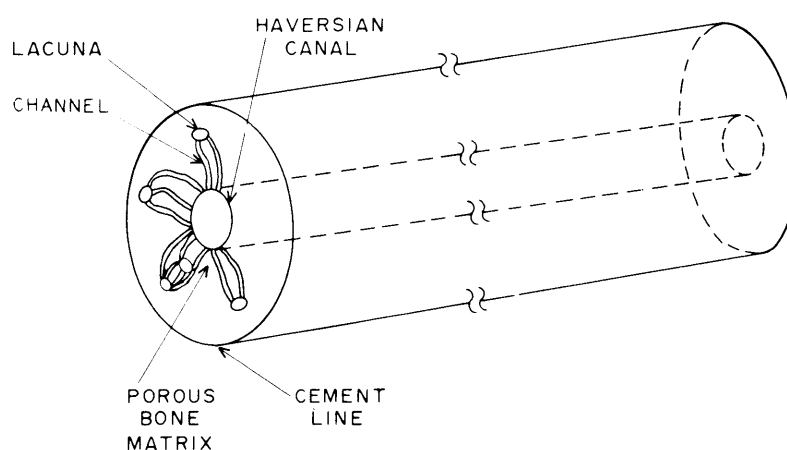


Fig. 1. Osteon model. Lacunae in the interior of the osteon are not shown for purposes of clarity. Channels are not shown to scale and all channels are not shown.

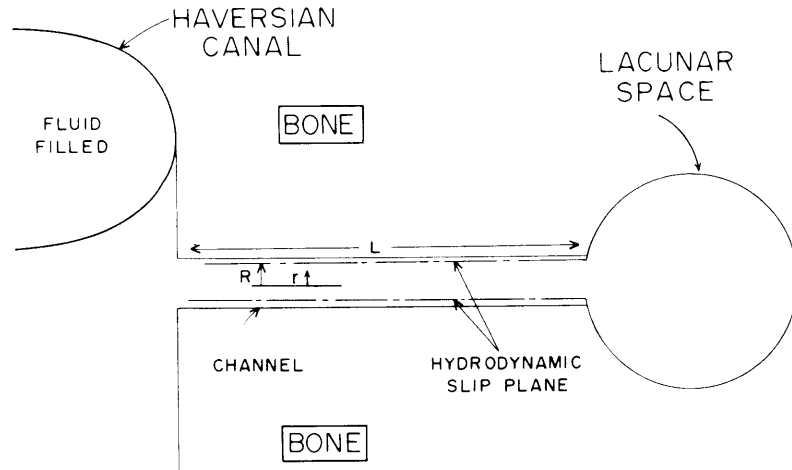


Fig. 2. Model of one of the cylindrical flow channels connecting a fluid filled lacunar space and Haversian canal. (Not shown to scale.)

defined as

$$\rho(r) = \sum_l z^l e C^l(r) \quad (1)$$

where $C^l(r)$ is the concentration of ion type l at the position r , e is the electronic charge, z^l is the valence of the l th ion type and the sum is over all ion types. For the monovalent ion system in this derivation, $z^l = \pm 1$. For equilibrium conditions, $C^l(r)$ is given by the Boltzmann distribution

$$C^l(r) = C_o^l \exp \left[\frac{-z^l e \phi(r)}{kT} \right] \quad (2)$$

where C_o^l is the equilibrium concentration of the l th ion type at the center of the channel, $\phi(r)$ is the electrical potential at r , k is Boltzmann's constant, and T is the absolute temperature. The potential and the charge density must also satisfy the Poisson equation

$$\nabla \cdot \{ \epsilon(r) \nabla \phi(r) \} = -\rho(r) \quad (3)$$

where $\epsilon(r)$ is the spatially dependent dielectric permittivity of the fluid. Assuming $\epsilon(r)$ is a constant, ϵ , and introducing equations (1) and (2) into equation (3), we obtain the Poisson-Boltzmann equation

$$\nabla^2 \phi(r) = \frac{-1}{\epsilon} \sum_l z^l e C_o^l \exp \left[\frac{-z^l e \phi(r)}{kT} \right] \quad (4)$$

Expanding the exponential above for $z^l e \phi(r)/kT \ll 1$ and retaining only the first two terms gives the linear form of equation (4)

$$\nabla^2 \phi(r) = \kappa^2 \phi(r) \quad (5)$$

where

$$\kappa^2 = \frac{e^2}{\epsilon kT} \sum_l (z^l)^2 C_o^l \quad (6)$$

where κ^{-1} is defined as the Debye length and charge neutrality at the center of the channel is assumed. The radial component of equation (5) in cylindrical coordinates is the modified Bessel equation of order zero, the

solution to which is

$$\phi(r) = C_1 I_o(\kappa r) + C_2 K_o(\kappa r) \quad (7)$$

$I_o(\kappa r)$ and $K_o(\kappa r)$ are the modified Bessel functions of the first and second kind, respectively. In equation (7), $C_2 = 0$ since $K_o(\kappa r)$ becomes infinite at $r = 0$. C_1 is evaluated using the boundary condition that at $r = R$ (the radius of the slip plane, as shown in Fig. 2), the potential $\phi(R) = Z$ where Z is the zeta potential. Therefore

$$C_1 = \frac{Z}{I_o(\kappa R)} \quad (8)$$

and

$$\phi(r) = \frac{Z I_o(\kappa r)}{I_o(\kappa R)} \quad (9)$$

Using equations (3), (5), and (9), we then obtain

$$\rho(r) = -\kappa^2 \epsilon Z \left[\frac{I_o(\kappa r)}{I_o(\kappa R)} \right] \quad (10)$$

Convective current flow in channels

When a stress is applied to bone, deformations in the matrix result in changes in the pressure in the lacunar and other spaces. Fluid flow must result through the channels connecting the lacunae to the Haversian canal (which remains at or near atmospheric or arterial pressure) and it is this flow which will be determined for the case shown in Fig. 2.

Assuming that the matrix is isotropic and elastic, that the fluid is Newtonian and that the lacunae are spherical fluid filled inclusions, for the case of uniaxial stress (such as obtained for the case of four-point bending), the dilatation of the lacunae can be computed as a function of the uniaxial stress. A step load results in an instantaneous dilatation of the inclusion, which is taken to be far from other inclusions in the matrix. Before fluid flow can occur, the instantaneous

dilatation, determined by Hashin (1969) is

$$\frac{\Delta V}{V} = \left[\frac{4\mu_1 + 3K_1}{4\mu_1 + 3K_w} \right] \frac{S}{3K_1} \quad (11)$$

where $\Delta V/V$ is the dilatation of the lacuna, μ_1 and K_1 are the shear and bulk moduli of the matrix, K_w is the bulk modulus of the fluid in the inclusion, and S is the uniaxial stress at a distance far from the inclusion. For pure bending, a stress gradient is developed across the sample. For purposes of this development, stress variations across an osteon are taken to be small and stress concentrations near the Haversian canal are neglected so that the intra-osteonal stress is effectively constant and uniaxial. The instantaneous pressure, P_o , in the inclusion (relative to a fluid reservoir exposed to the atmosphere or the arterial system) resulting from $\Delta V/V$ is

$$P_o = -K_w \frac{\Delta V}{V} = -\frac{K_w}{3K_1} \left[\frac{4\mu_1 + 3K_1}{4\mu_1 + 3K_w} \right] S. \quad (12)$$

The sign of P_o is taken as positive when S is compressive and negative when S is tensile. This result is the same as that obtained by Jendrucko *et al.* (1976) when $K_w \rightarrow \infty$, i.e., an incompressible fluid, and differs from their result for a compressible fluid by a geometric argument since they had modelled a cylindrical inclusion in a state of plane stress. For the case of an incompressible fluid, equation (12) reduces to

$$P_o = \frac{-1}{9K_1} (4\mu_1 + 3K_1) S. \quad (13)$$

There are a number of channels associated with each lacuna through which fluid can flow to the Haversian canal. These channels will, in general, include canaliculi and the interconnected porous regions of the matrix. The exact radii, lengths and numbers of these channels are not known. Estimates by Johnson *et al.* (1982) suggest that the canaliculi may be partially blocked by cell debris, in the case of machined specimens, making a determination of the effective radius difficult. Certainly, in living bone, the canaliculi contain cell processes resulting in effective radii for fluid flow that are much smaller than the anatomical radii of approximately 0.1μ . The porous channels of the matrix are on the order of 0.01μ radius or smaller, however, the path lengths and number cannot be evaluated simply.

In view of the above, we will assume that the i th lacuna can be modelled as an initial lacunar volume, V_o , drained by a system of n_i rigid fluid channels with effective radius R_i and length L_i . Assuming Poiseuille flow in the channels, the volume of fluid per unit time, Q , flowing in all of the n_i channels, for the i th lacuna, is

$$Q = \left[\frac{n_i \pi R_i^4}{8\eta L_i} \right] P \quad (14)$$

where η is the fluid viscosity and P is the time dependent pressure difference between the lacuna and the Haversian canal. Poiseuille flow is assumed despite

the limited compressibility of the fluid and the surface roughness of the channels. The compressibility of the fluid and the flow out from the lacuna account for changes in the lacunar volume, dV/dt

$$\frac{dV}{dt} = \frac{-V_o}{K_w} \left(\frac{dP}{dt} \right) + \left[\frac{n_i \pi R_i^4}{8\eta L_i} \right] P. \quad (15)$$

Clearly, as the fluid leaves the lacuna, the pressure decreases and reaches zero when the total volume dilatation reaches the value it would have had if the lacuna had been an empty cavity. We can define an effective bulk modulus, K_{eff} , for this period of fluid flow, such that

$$\frac{1}{K_{eff}} \equiv \frac{-1}{V_o} \left(\frac{dV}{dP} \right) \quad (16)$$

where the total volume change is taken to be small compared to the initial lacunar volume. Rearranging equation (16) and dividing through by dt gives

$$\frac{dV}{dt} = \frac{-V_o}{K_{eff}} \left(\frac{dP}{dt} \right) \quad (17)$$

and with equation (15)

$$V_o \left[\frac{K_w - K_{eff}}{K_w K_{eff}} \right] \left(\frac{dP}{dt} \right) + \left[\frac{n_i \pi R_i^4}{8\eta L_i} \right] P = 0. \quad (18)$$

Solving for P

$$P = P_o \exp \left\{ \left[\frac{-n_i \pi R_i^4}{8\eta L_i V_o} \right] \left[\frac{K_w K_{eff}}{K_w - K_{eff}} \right] t \right\} \quad (19)$$

where P_o is the initial pressure given by equation (12). K_{eff} can be readily evaluated by inserting equation (19) in equation (15), integrating over all time, and equating the resulting change in volume to that obtained from equation (11) in the limiting case of an empty cavity for which $K_w/K_1 \rightarrow 0$. The result is

$$K_{eff} = \frac{4\mu_1 K_w}{8\mu_1 + 3K_w}. \quad (20)$$

Inserting equation (20) into equation (19) gives

$$P = P_o \exp(-t/\tau_i) \quad (21)$$

where τ_i is

$$\tau_i = \left[\frac{2\eta L_i V_o}{\pi n_i R_i^4} \right] \left[\frac{4\mu_1 + 3K_w}{\mu_1 K_w} \right]. \quad (22)$$

The convective electrical current, j_{ci} , in each channel is given by

$$j_{ci} = \int_0^{R_i} \rho(r) v(r) 2\pi r dr \quad (23)$$

where $\rho(r)$ is given by equation (10) and $v(r)$ is the radially dependent fluid velocity in each channel and is assumed to be given by Poiseuille's equation

$$v(r) = \frac{P}{4\eta L_i} (R_i^2 - r^2) \quad (24)$$

where P is given by equations (21) and (22). Integrating

equation (23) gives:

$$j_{ci} = \left[\frac{-Z\pi\epsilon R_i^2}{\eta L_i} \right] \left[\frac{I_2(\kappa R_i)}{I_0(\kappa R_i)} \right] P_o \exp(-t/\tau_i) \quad (25)$$

where $I_2(\kappa R_i)$ is the modified Bessel function of order 2.

Determination of streaming potentials

Equation (25) is the convective current flow between the *i*th lacuna and the Haversian canal through one of the flow channels. The total convective current will be the sum of the currents for all of the channels and from all of the lacunae in the osteon. The exact expression will, of course, depend upon the location of the lacunae which will affect the value of L_i , the length of the channels. For simplicity, we will first model the osteon as having lacunae that occur uniformly in two concentric cylinders (shells) of radius a_1 and a_2 ($a_1 < a_2$) with N_1 identical lacunae at a_1 and N_2 identical lacunae at a_2 , as shown in Fig. 3. This will later be generalized. We will consider that each lacunae is drained by n channels of radius r . The total convective current density across the cylindrical surface of radius u (for $u < a_1$) is then

$$\left[\frac{n}{2\pi u h} (N_1 j_{c1} + N_2 j_{c2}) \right]$$

where j_{c1} and j_{c2} are given by equation (25) and h is the length of the osteon. The conduction current density, J , flowing across this cylindrical surface at u is in the opposite direction and is given by $J = \sigma E_u$ where E_u is the radially directed electric field and σ is the conductivity of the bone-fluid system. Classical streaming potential theory equates these two currents and thereby determines the steady state electric field generated by electrokinetic mechanisms. We will determine the time dependence of the field E_u and examine the conditions that result in achieving steady state.

The difference between the convective and conductive currents is equal to the rate of change of charge,

dq/dt , within the cylinder of radius u

$$(dq/dt) = n(N_1 j_{c1} + N_2 j_{c2}) - 2\pi\sigma E_u u h. \quad (26)$$

Since E_u is given by Gauss's law

$$2\pi u h E_u = \frac{q}{\epsilon_s} \quad (27)$$

where ϵ_s is the permittivity of the bone-fluid system, we can write

$$(dE_u/dt) = \frac{1}{2\pi u h \epsilon_s} (dq/dt). \quad (28)$$

With equation (26), equation (28) becomes

$$(dE_u/dt) + \frac{\sigma}{\epsilon_s} E_u = \frac{n}{2\pi \epsilon_s u h} (N_1 j_{c1} + N_2 j_{c2}). \quad (29)$$

Solving for E_u and noting the explicit time dependence of j_{c1} and j_{c2} as given in equation (25)

$$E(u, t) = \frac{-ZR^2 n P_o}{2\eta u \epsilon_s} \left[\frac{I_2(\kappa R)}{I_0(\kappa R)} \right] \left\{ \frac{N_1}{h L_1} \left[\frac{1}{\frac{\sigma}{\epsilon_s} - \frac{1}{\tau_1}} \right] \times \left[\exp\left(\frac{-t}{\tau_1}\right) - \exp\left(\frac{-\sigma t}{\epsilon_s}\right) \right] + \frac{N_2}{h L_2} \left[\frac{1}{\frac{\sigma}{\epsilon_s} - \frac{1}{\tau_2}} \right] \times \left[\exp\left(\frac{-t}{\tau_2}\right) - \exp\left(\frac{-\sigma t}{\epsilon_s}\right) \right] \right\} \quad (30)$$

where τ_1 and τ_2 are given by equation (22) for R_i equal to R and L_i equal to L_1 and L_2 , respectively. All other parameters are as previously defined. Equation (30) can be generalized for more than two concentric shells of lacunae, all of which are at radii greater than u . Under these conditions, each shell will be characterized by an effective length L_k and a time constant τ_k . This

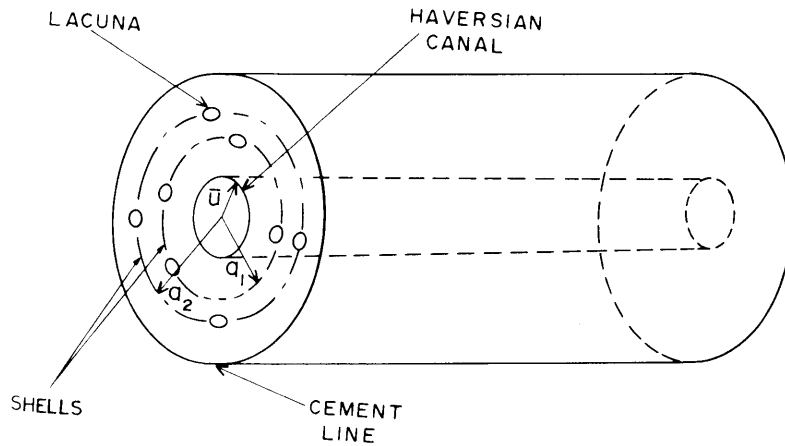


Fig. 3. Osteon model depicting two shells of lacunae at radii a_1 and a_2 . Shells not shown in interior of osteon.

gives

$$E_u(u, t) = \frac{-ZR^2 n \epsilon P_o}{2\eta u \epsilon_s} \left[\frac{I_2(\kappa R)}{I_o(\kappa R)} \right] \sum_k \frac{N_k}{hL_k} \left[\frac{1}{\frac{\sigma}{\epsilon_s} - \frac{1}{\tau_k}} \right] \times \left[\exp\left(\frac{-t}{\tau_k}\right) - \exp\left(\frac{-\sigma t}{\epsilon_s}\right) \right] \quad (31)$$

where the sum over k is the sum over the number of concentric lacunar shells greater than u and N_k/h is the number of lacunae on the k th shell per unit length of the osteon. The electrical potential, $\phi(u, t)$, within the osteon is then determined by integrating equation (31) from the radius of the Haversian canal, \bar{u} , to u

$$\phi(u, t) = \frac{ZR^2 n \epsilon P_o}{2\eta \epsilon_s} \left[\frac{I_2(\kappa R)}{I_o(\kappa R)} \right] \int_{\bar{u}}^u \left\{ \sum_k \frac{N_k}{hL_k u} \left[\frac{1}{\frac{\sigma}{\epsilon_s} - \frac{1}{\tau_k}} \right] \times \left[\exp\left(\frac{-t}{\tau_k}\right) - \exp\left(\frac{-\sigma t}{\epsilon_s}\right) \right] \right\} du. \quad (32)$$

This equation can be further simplified by assuming $\sigma/\epsilon_s \gg 1/\tau_k$ (Johnson *et al.*, 1980). τ_k is numerically evaluated in the Discussion section of this paper. The conductive term, σ/ϵ_s , is on the order of 10^6 s^{-1} (Chakkalal *et al.*, 1980; Kosterich *et al.*, 1983) while the maximum value of $1/\tau_k$ is on the order of 10^3 s^{-1} . Thus, the conduction current establishes steady state conditions with the convective current instantaneously and the final expression for the intra-osteonal streaming potential is

$$\phi(u, t) = \frac{Z\epsilon}{4\pi\sigma\eta} P_{eff}(u, t) \quad (33)$$

where

$$P_{eff}(u, t) = 2\pi n R P_o \left[\frac{I_2(\kappa R)}{I_o(\kappa R)} \right] \times \int_{\bar{u}}^u \left\{ \sum_k \frac{N_k}{hL_k u} [\exp(-t/\tau_k)] \right\} du. \quad (34)$$

Equation (33) has the form of a classical streaming potential (Shaw, 1969), with an effective pressure given by equation (34). Equations (33) and (34) must be evaluated numerically (see Discussion section) since the sum over k in equation (34) contains an implicit function of u . This is derived from the u dependence of N_k , L_k , and τ_k , each of which are model dependent.

DISCUSSION

Limitations of the theory

We have developed a model characterizing electrokinetics within a single osteon. The development is subject to several limitations which must be addressed to define the realm of application for the proposed theory.

The Boltzmann distribution (equation 2) describes

the radial concentration of the l th species as a function of the electrostatic potential. Explicit in this application of the Boltzmann distribution is that the potential is zero at the center of the channel ($r = 0$). This condition is obtained when the Debye length is small compared to the radius of the channel. Conversely, the Debye length must be greater than the interionic distance in order for the continuum approximation implicit in the Poisson-Boltzmann equation to apply. These will impose upper and lower boundaries for the radius of the channels and the ion concentrations for which this formalism is valid.

The linearization of equation (4) is also a limitation to the present development. Expansion of the exponential in equation (4) dictates that $z'e\phi/kT \ll 1$. This approximation is valid in bone where, here, the largest absolute value of ϕ is the value of the zeta potential which is on the order of 10 mV. Dukhin and Derjaguin (1974) reveal insight into numerical solutions for the cylindrical form of the Poisson-Boltzmann equation.

Another complication of the theory deals with the exact location of the slip plane within the channel. The distance from the channel wall to the slip plane must be small compared to the radius of the channel for fluid to flow freely in the central portion of the channel. These distances are unknown for the irregular and complex fluid channels of bone, but distances on the order of several Angstroms seem appropriate and this was implicitly assumed.

The zeta potential at a *real* solid-fluid interface depends upon the geometry of the interface, the precise surface charge distribution on the solid surface, the presence of adsorbed ion species and their locations at the interface, and the spatial distribution of charge in the fluid. It is also influenced by the presence of charged macromolecules at the interface. All of these conditions may be expected to vary from one channel to another and possibly from one region of a channel to another region in the same channel. In any given electrokinetic experiment, some average value of the zeta potential is observed. In this calculation, the zeta potential is taken to be a constant 'average' value for all channels of fluid flow, thus eliminating the above complexities from the analysis.

In light of the formalism adopted from Hashin (1969), the matrix surrounding the lacuna is assumed to be elastic. Gottesman and Hashin (1980) note that the viscoelastic collagen fibrils are embedded in elastic hydroxyapatite crystals, so that the assumption of an elastic matrix is appropriate. Nevertheless, slight viscoelastic properties of the matrix will introduce time dependent terms in equation (12).

Functional dependencies

There are several functional dependencies of the predicted potentials and relaxation times which relate to experimental results on a micro-scale (within a single osteon) and on a macro-scale (spanning tens of osteons). These will now be reviewed.

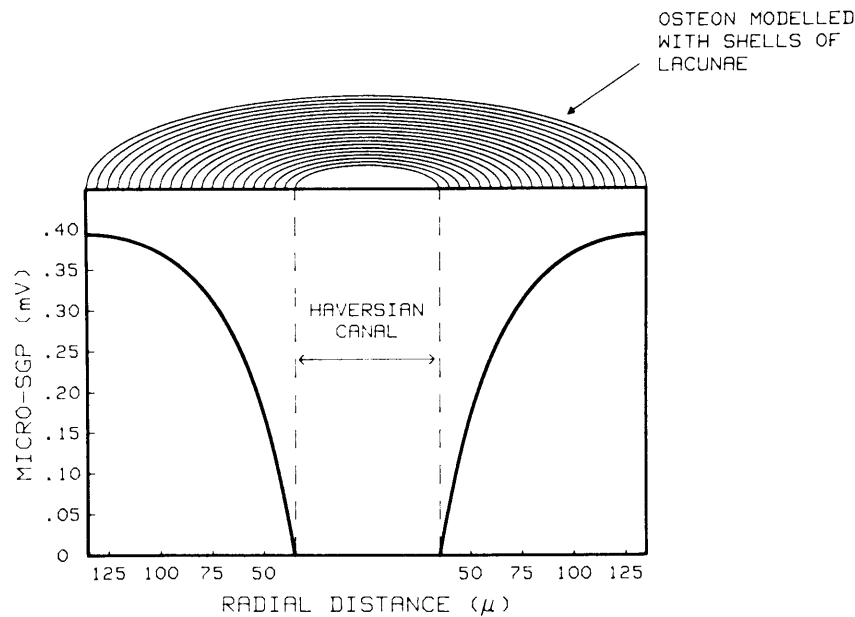


Fig. 4. Predicted intra-osteonal potential profile for a state of uniaxial compressive stress. (Equations 33 and 34.)

The radial dependence of the intra-osteonal potential is given in equations (33) and (34). The integral cannot be performed analytically since N_k , L_k and τ_k have an implicit radial dependence. The integral can be evaluated numerically. (The exact details of this numerical analysis can be found in a subsequent portion of this section.) The resulting radial dependence is shown in Fig. 4, for the case when S is a uniaxial compressive stress. The inverse is obtained for a state of uniaxial tensile stress. The potential profile is shown to increase radially, independent of direction within the osteon. The slope of the potential profile (the negative of the electric field) is a maximum adjacent to the Haversian canal and decreases radially toward the cement line. This is in excellent agreement with experimental microelectrode results reported in Figs 4 and 5 of Starkebaum *et al.* (1979). Furthermore, Starkebaum *et al.* (1979) report that for the case of symmetric osteons, the potentials near the Haversian canal satisfy a $\ln(u/\bar{u})$ relationship. The potential profile depicted in Fig. 4 can be fit to the relationship

$$\phi(u, t \rightarrow 0) = 0.014 + 0.42 \ln(u/\bar{u}) \quad (\text{mV}) \quad (35)$$

with a 0.98 correlation for radial distances out to twice the Haversian canal radius (\bar{u}). The coefficient of the \ln term in equation (35) compares well with the value reported by Starkebaum *et al.* (1979) of 0.62 ± 0.21 mV.* This coefficient is independent of the spacing of the shells for spacings of up to 5μ per shell.

The amplitude of the cusp depends linearly upon the

*The authors note a misprint in Starkebaum *et al.* (1979). The coefficient of the logarithmic term is in millivolts, not volts.

uniaxial stress. For a four-point bending experiment, the uniaxial stress is proportional to the distance between the osteon center and the neutral axis of bending. Therefore, the cusp amplitude (or, equivalently, the electric field amplitude near the Haversian canal) is predicted to be a linear function of the osteon position relative to the neutral axis and this is in good agreement with the experimental results of Starkebaum *et al.* (1979).

Equation (34) predicts that the potential will be inversely proportional to both the fluid viscosity and the conductivity of the bone-fluid system. The dependence of micro-SGP on fluid viscosity has not been determined experimentally. A macroscopic anatomical model has not been developed but the same functional dependence on viscosity ought to be evident for both the macroscopic and microscopic cases. Gross and Williams (1982) and Pienkowski and Pollack (1983) report that the amplitude of the macroscopic SGPs are inversely proportional to the viscosity of the fluid, as predicted by this model.

Chakkalakal *et al.* (1980) and Kosterich *et al.* (1983, 1984) have investigated the dielectric properties of macroscopic samples of cortical bone. Both groups report that the conductivity of the bone-fluid system is 0.5–1% of the conductivity of the steeping fluid. Thus, studies of the dependence of the amplitude of SGPs on the conductivity of the steeping solution will test the functional dependence predicted in equation (33). Gross and Williams (1982) and Pienkowski and Pollack (1983) have shown the macro-SGP amplitude is indeed inversely proportional to the steeping fluid conductivity and the latter group has also shown this on a micro-scale. Pollack *et al.* (1983) have also

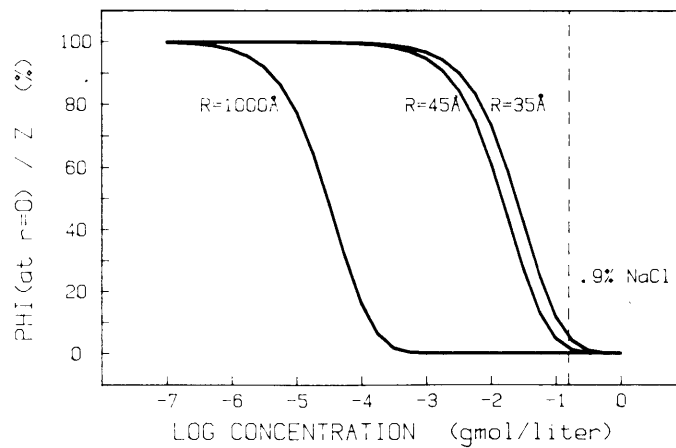


Fig. 5. Predicted potential, $\phi(r)$, at center of channel shown as a percentage of the zeta potential for various solution concentrations and channel radii. (Equation 9.)

proposed that the zeta potential of bone may vary with ion concentration of the steeping solution and, hence, the conductivity.

Equation (22) gives an expression for τ_k , the relaxation time associated with the k th shell of lacunae. This expression is in essential agreement with that determined by Johnson *et al.* (1982). Experimental values for the microscopic relaxation times have not been reported but, again, the functional dependence of both the microscopic and macroscopic decay times on viscosity and conductivity should be the same. Interpretation of single osteon model parameters such as L_k , N_k , n and R from macroscopic data is inappropriate since the decay times are highly dependent on the specific fluid channel geometries. The macroscopic results for τ_k of Gross and Williams (1982) and Pienkowski and Pollack (1983) reveal the linear proportionality between the decay times and the viscosity. The latter group has shown this relationship to hold with a correlation coefficient of 0.96. Both groups also found that τ_k are independent of solution conductivity, for several decades of variation of conductivity. Both findings are in agreement with equation (22). This would not be predicted if the stress generated potentials were piezoelectric in origin.

One further result of this work accounts for multiple relaxation times associated with the decay of the potential. This is seen in equation (22) in the dependence of τ_k on L_k , the effective length of the channel from the k th lacuna to the Haversian canal. L_k will vary within an osteon and this will result in multiple time constants. A similar effect may account for the multiple time constants reported on the macro-scale though micro-SGP relaxation must be investigated.

Numerical analysis

The final expressions for the anatomic model for streaming potentials in osteons is based on many

parameters which may be numerically evaluated, using typical reported values. The average radius of the channel (R) through which the streaming fluid flows and the average number (n) of these channels are not known, but this evaluation will give insight into numerical values and their anatomical significance.

We will consider a cylindrical osteon with outer radius of 135μ , an Haversian canal radius (\bar{u}) of 35μ , and a length (h) of 1000μ . Considering that there is one lacuna for each $77,000 \mu^3$ (Boyde, 1972), there are 700 lacunae in the osteon. Each lacuna is taken to be spherical and of radius of 10μ . We will use a continuous model for the distribution of the shells of lacunae such that the shells are one micron apart, beginning next to the Haversian canal and ending next to the cement line. The total number of lacunae are taken to be evenly distributed on the total area of these shells. Therefore, the number of lacunae on shell k (N_k) is proportional to the shell radius. We estimate the effective length of the flow channel (L_k) to be the distance from the k th shell to the Haversian canal.

Using the following mechanical properties for wet cortical bovine bone

$$\mu_1 = 0.7 \times 10^{11} \text{ g cm}^{-1} \text{ s}^{-2} \text{ from Frasca } et al. (1981)$$

$$K_1 = 1.5 \times 10^{11} \text{ g cm}^{-1} \text{ s}^{-2}$$

$$K_w = 0.22 \times 10^{11} \text{ g cm}^{-1} \text{ s}^{-2}$$

$S = -4.8 \times 10^8 \text{ g cm}^{-1} \text{ s}^{-2}$ from Starkebaum *et al.* (1979) for the case of maximum compression in their work.

P_0 , the initial lacunar pressure before any fluid flow, is $5 \times 10^7 \text{ g cm}^{-1} \text{ s}^{-2}$.

Considering the steeping fluid to be physiological saline (0.9% NaCl), the Debye length (at 25°C) is 8 \AA which approaches the interionic spacing. The conductivity of the bone-fluid system is taken as $0.007/\Omega\text{-m}$ (Chakkalakal *et al.*, 1980) and the zeta potential is

taken as -10 mV (Eriksson, 1976). The viscosity and the dielectric permittivity are taken to be that of physiological saline, $0.01 \text{ g cm}^{-1} \text{ s}^{-1}$ and $75.34\epsilon_0$, respectively.

We will evaluate the peak electric field developed at the Haversian canal and compare this to the experimental results of Starkebaum *et al.* (1979) who report that the peak field for 1 Hz sinusoidal loading is 14 V/m. Using equation (31) for $\sigma/\epsilon_s \gg 1/\tau_k$

$$E(\bar{u}, t \rightarrow 0) = 1.01 \times 10^{15} nR^2 \left[\frac{I_2(\kappa R)}{I_0(\kappa R)} \right] (\text{V/m}^3) \quad (36)$$

and for $E = 14$ V/m, we find

$$nR^2 \left[\frac{I_2(\kappa R)}{I_0(\kappa R)} \right] = 1.4 \times 10^{-14} (\text{m}^2). \quad (37)$$

Using equation (37) in equations (33) and (34), the peak intra-osteonal potential is determined numerically to be approximately 0.40 mV, which is the same order of magnitude of that reported by Iannacone *et al.* (1979), Starkebaum *et al.* (1979), and Pienkowski and Pollack (1983). Figure 4 numerically illustrates the intra-osteonal potential profile.

The quantities n and R in equation (37) may be estimated under the following two limiting conditions:

(1) Anatomically, the largest channels connected to the lacuna are the canaliculi with an average radius of 1000 Å (Table 1). Using this value, the predicted number of channels is roughly 1.5. Johnson *et al.* (1982) point out that the canaliculi may be clogged by cell debris and other particulate matter. Certainly, in living bone, cell processes lie within the canaliculi and occlude a significant portion of the channel. In either case, this would result in smaller radii for the fluid flow channels, and increase their predicted number, thus closer to the anatomical number of canaliculi (30–50 per lacuna).

(2) Electrostatically, the smallest radius must be such that the potential remains zero at the center of the channel. Figure 5 shows the predicted value of the potential at the center of the channel relative to the zeta potential (equation 9) for three radii: 1000, 45 and 35 Å. For radii less than 45 Å, the potential at the center of the channel is no longer zero at 0.9% NaCl and the form of the Boltzmann distribution used in equation (2) is no longer valid. We will use a lower limit of 45 Å for the value of the radius and the resulting number of channels, from equation (37), is 10^3 . This anatomically corresponds to the porous fraction of the bone (Table 1) and indicates that approximately 0.005% of the surface of the lacuna is open to these pores through which the fluid flows.

This analysis cannot distinguish between flow in canaliculi, whether clogged or not, or flow in the porous fraction of bone. Based on these considerations, the flow through such channels does result in very small Reynolds numbers and indicates a laminar flow regime.

The relaxation times associated with these values of

the radius can be evaluated from equation (22). We will consider an average value of L_k of 35 microns. For $R = 1000$ Å, τ_k is on the order of 10^{-3} s. For $R = 45$ Å, τ_k is on the order of 10^{-1} s. At this time, values for the relaxation times of intra-osteonal potentials have not been reported. Values for macroscopic relaxation times (Gross and Williams, 1982; Pienkowski and Pollack, 1983) are from 10^{-1} to 1 s, however these values may not be directly compared to intra-osteonal values. Nevertheless, if the longer time constants (10^{-1} s) are observed for single osteons, the smaller radius channels would be responsible for fluid flow.

CONCLUSIONS

The theory for streaming potentials presented here is based upon a reasonable anatomical model and upon first principles of electrokinetic theory and continuum mechanics. Many of the previously published observations of potentials in osteons and across macroscopic specimens are explained for the first time in terms of such a model. The cusp-like behavior of intra-osteonal potentials is explained, the dependence of potentials on solution viscosity and conductivity is demonstrated, and insight is gained relative to the time dependence of stress generated electrical effects.

Acknowledgement—The authors acknowledge with great appreciation the support of the National Science Foundation (Grant numbers INT 81-8481 and ECS 80-17856) and the Bulgarian Academy of Sciences for their continued support throughout this collaborative study.

REFERENCES

- Anderson, J. and Eriksson, C. (1970) Piezoelectric properties of dry and wet bone. *Nature* **227**, 491–492.
- Boyd, A. (1972) Scanning electron microscope studies of bone. *The Biochemistry and Physiology of Bone*. Vol. 1 (Edited by Bourne, G. H.), pp. 259–310. Academic Press, New York.
- Chakkalakal, D. A., Johnson, M. W., Harper, R. A. and Katz, J. L. (1980) Dielectric properties of fluid-saturated bone. *IEEE Trans. Biomed. Engng* **27**, 95–100.
- Dukhin, S. S. and Derjaguin, B. V. (1974) Equilibrium double layer and electrokinetic phenomena. *Surface and Colloid Science*. Vol. 7 (Edited by Matijevic, E.), pp. 49–272. John Wiley, New York.
- Eriksson, C. (1976) Bone morphogenesis and surface charge. *Clin. Orthop.* **121**, 295–302.
- Frasca, P., Harper, R. and Katz, J. L. (1981) Strain and frequency dependence of shear storage modulus for human single osteons and cortical bone microsamples—size and hydration effects. *J. Biomechanics* **10**, 679–690.
- Gottesman, T. and Hashin, Z. (1980) Analysis of viscoelastic behaviour of bones on the basis of microstructure. *J. Biomechanics* **13**, 89–96.
- Gross, D. and Williams, W. S. (1982) Streaming potential and the electromechanical response of physiologically moist bone. *J. Biomechanics* **15**, 227–295.
- Hashin, Z. (1969) The inelastic inclusion problem. *Int. J. Engng Sci.* **7**, 11–36.
- Iannacone, W., Korostoff, E. and Pollack, S. R. (1979) Microelectrode studies of stress generated potentials obtained from uniform and nonuniform compression of human bone. *J. Biomed. Mat. Res.* **13**, 753–763.
- Jendrucko, R. J., Hyman, W. A., Newell, P. H. and

- Chakraborty, B. K. (1976) Theoretical evidence for the generation of high pressure in bone cells. *J. Biomechanics* **9**, 87-91.
- Johnson, M. W., Chakkalakal, D. A., Harper, R. A. and Katz, J. L. (1980) Comparison of the electromechanical effects in wet and dry bone. *J. Biomechanics* **13**, 437-442.
- Johnson, M. W., Chakkalakal, D. A., Harper, R. A., Katz, J. L. and Rouhana, S. W. (1982) Fluid flow in bone *in vitro*. *J. Biomechanics* **15**, 881-885.
- Kosterich, J. D., Foster, K. R. and Pollack, S. R. (1983) Dielectric permittivity and electrical conductivity of fluid saturated bone. *IEEE Trans. Biomed. Engng* **30**, 81-86.
- Kosterich, J. D., Foster, K. R. and Pollack, S. R. (1984) Dielectric properties of fluid saturated bone: effect of variation in conductivity of immersion fluid. *IEEE Trans. Biomed. Engng* **31**, 369-374.
- Overbeek, J. Th. G. (1952) Electrochemistry of the double layer. *Colloid Science* (Edited by Kruyt, H. R.), pp. 115-193. Elsevier, Amsterdam.
- Piekarski, K. and Munro, P. (1977) Transport mechanisms operating between blood supply and osteocytes in long bones. *Nature* **269**, 80-82.
- Pienkowski, D. and Pollack, S. R. (1983) The origin of stress generated potentials in fluid saturated bone. *J. Orthop. Res.* **1**, 30-41.
- Pollack, S. R., Salzstein, R. and Pienkowski, D. (in press) Streaming potentials in fluid filled bone. *Ferroelectrics*.
- Shaw, D. (1969) *Electrophoresis*. Academic Press, New York.
- Starkebaum, W. S., Pollack, S. R. and Korostoff, E. (1979) Microelectrode studies of stress generated potentials in four point bending of bone. *J. Biomed. Mat. Res.* **13**, 729-751.